Stabilized Combustion of Circular Fuel Duct with Liquid Oxygen

Ayumu Tsuji[a,*], Yuji Saito[b], Landon Kamps[c], Masashi Wakita[c], Harunori Nagata[c]

[a]*Graduate School of Engineering, Hokkaido University, 8 Nishi, Kita13-jo, Kita-ku, Sapporo, Hokkaido 060-8628, Japan*
[b]*Department of Aerospace Engineering, Tohoku Univeristy, Sendai, Miyagi 980-8579, Japan*
[c]*Faculty of Engineering, Hokkaido University, Nishi 8, Kita 13-jo, Kita-ku, Sapporo, Hokkaido 060-8628, Japan*

Abstract

This research is an investigation of the flame spread opposed to a liquid oxidizer flow in a solid fuel duct. Several firing tests were conducted using liquid oxygen as the oxidizer and solid poly methyl methacrylate (PMMA) as the fuel. The results indicate that the flame spread rate decreased with increasing oxidizer port velocity and decreasing port diameter. This study reveals through visual confirmations and empirical correlations of the flame spread rate that the flame spread opposed to liquid oxygen in a solid fuel duct can be classified as stabilized combustion. Extinction and abnormal regression were observed when oxidizer port velocity was high and port diameter was small. Furthermore, the cooling of the solid fuel by the liquid oxygen flow had a strong effect on the transition between normal regression and extinction, or abnormal regression. A model of the flame spread rate which considers the heat balance at the fuel surface assuming a fully developed thermal boundary layer is introduced and shown to agree well with the experimental results. Lastly, it is revealed that the difference in kinematic viscosity between liquid oxygen and gaseous oxygen is the main reason dependency of port diameter on flame spread rates differs between the liquid oxygen tests in this study and gaseous oxygen tests in previous studies.

Keywords:
Stabilized combustion, Flame spread, Solid Fuel, Liquid oxidizer, Flame spread rate modeling

4357 words

*Corresponding author:
Email address:
a.tsuji_spacesys@frontier.hokudai.ac.jp (Ayumu Tsuji)

1. Introduction

The axial-injection end-burning hybrid rocket using gaseous oxidizer has attracted the attention of prominent hybrid rocket researchers for its desirable combustion characteristics, high fuel regression rates, and throttling capability [1, 2]. This type of hybrid rocket uses a cylindrical solid fuel with a dense array of submillimeter diameter ports running in the axial direction. Gaseous oxidizer is passed through the port array, and a diffusion flame forms at each port exit, a phenomenon which is referred to as stabilized combustion.

It is impractical to load and store gaseous oxidizer in a rocket intended to be used as the propulsion system for an earth launch vehicle because the tank required to store the oxidizer would be unreasonably large and heavy. For these reasons, axial-injection end-burning hybrid rocket-powered launch vehicles will require the use of a liquid oxidizer. However, the authors are not aware of any previous research on the stabilized combustion of a liquid oxidizer in a solid fuel port. It is necessary to further clarify the characteristics of the heterogenous combustion of a liquid oxidizer and solid fuel, as a first step towards a viable technique, specifically regarding the phenomenon of stabilized combustion.

Previous researchers have investigated the flame spread opposed to gaseous oxidizer flow over a combustible solid: notably Lastrina et al. [3] and Fernandez-Pello et al. [4]. Building on those results, Hashimoto et al. and Matsuoka et al. experimentally investigated flame spread opposed to gaseous oxidizer flow in a circular fuel duct [5, 6]. Hashimoto and Matsuoka et al. reported that stabilized combustion is formed when oxidizer port velocity exceeds a certain value and mentioned that the following three characteristics are essential for attaining stabilized combustion: fuel regression rate in the axial direction coinciding with flame spread rate, low flame spread rate, and enlarging port diameter. As far as we know, there has only been one report about the flame spread opposed to liquid oxidizer. In a recent study by Takei et al. a few firing tests were conducted in which liquid oxygen was passed through a multiport PMMA fuel grain placed within a rocket chamber, however the discussion of results was limited to the fuel regression shape at the end of firing and the feasibility of such a configuration as a gas generator [7]. Their research did not sufficiently examine the relation between oxidizer port velocity, port diameter, ambient pressure and flame spread rate, which is important for the design of axial-injection End-Burning hybrid rockets. For this reason, most of the combustion characteristics of liquid oxidizer and solid fuel are still unknown. The purpose of this study is to reveal the characteristics of flame spread opposed to liquid oxidizer flow in a circular fuel duct by observing the combustion directly, with the specific aim of understanding the influence of port diameter and oxidizer port velocity on flame spread rate, and constructing a model that includes key mechanisms of the combustion.

2. Experimental procedure and apparatus

Fuel port sizes vary from 1.0, 2.0, 3.0 and 6.0 mm in diameter. All fuel grains except for the 6.0 mm port diameter fuel grains were prepared in-house by drilling a cylindrical port through the center of a rectangular prismatic rod with outer dimensions of $20 \times 30 \times 7$ mm. Rectangular prismatic rods were preferred as a source material because they provide a clear field of view of the flame front from the side. The 6.0 mm port diameter fuel grains were made from pre-manufactured tubes with an outer diameter of 12.0 mm because the port diameter accuracy would not have been acceptable had the ports been made in the rectangular rods with the drill available.

Oxidizer port velocity was held constant during each test but ranged from 1 to 7 m/s between tests. The length of the port is too short for the complete development of the turbulent velocity boundary layer, but the length is enough for preventing the occurrence of two-phase flow. Figure 1 shows the experimental apparatus. All tests were conducted under atmospheric pressure. As shown in the upper left of Fig. 1, fuel was mounted vertically in the downward direction in a rectangular duct through which gaseous nitrogen flows downward. Nitrogen gas is passed through the duct to prevent frosting on the fuel surface and maintain a clear view of the flame front. Before firing, an insulated reservoir storing the liquid oxygen was decompressed to approximately 0.03 MPa by vacuum pump to cool it from 90 K to 80 K. This was another measure taken to prevent the liquid oxygen from changing phase on the way to the fuel. Gaseous helium was used as a pressurant to feed the liquid oxygen through an orifice and feed line, which was insulated, and cooled by liquid nitrogen, to the fuel port. Fuel was ignited from the downstream end of the port by burning incense while liquid oxygen was being passed through the fuel. Gaseous nitrogen was used to extinguish the flame after stopping the liquid oxygen supply. The oxygen mass flowrate was measured by the pressure drop between the reservoir and the fuel upstream position. The combustion and fuel regression

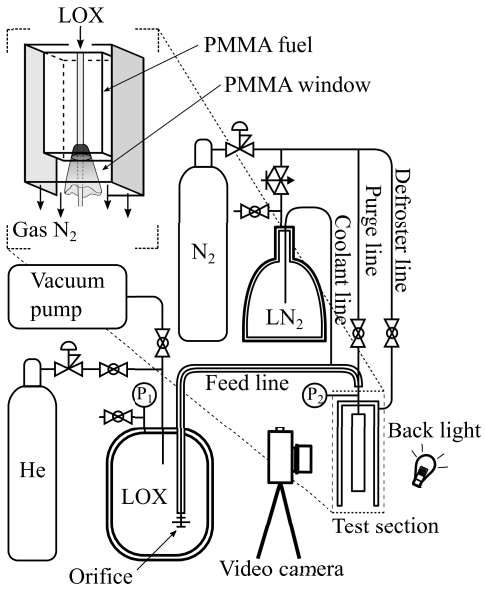

Fig. 1. Schematic of the experimental apparatus.

were observed and recorded by digital video camera using the back-light method, and the opposed flow flame spread rate was determined by visually identifying the flame position between frames. A high-speed camera (Photron FASTCAM SA3 model 120K-M3) was used to confirm whether the oxygen flow was in a fully liquid phase or in a state of two-phase flow, as well as to observe the leading edge of fuel regression.

3. Results and discussion

3.1. Flame spread rate

Figure 2 shows images of the combustion and fuel regression shapes for port diameters of 1.0, 2.0, 3.0 and 6.0 mm. Most liquid oxygen passes through the diffusion flame without being vaporized, which suggests that the diffusion flame is formed along the regressing fuel wall surface and is a frustum in shape, with liquid oxygen passing through the center of it. Although a small amount of liquid oxygen vaporizes near the vicinity of the diffusion flame, the high-speed camera shows that oxygen is entirely in the liquid phase up to the port exit in all experiments. In addition, fuel regression profile was bell-shaped. This is because the diffusion flame regressed the fuel in both the axial and radial directions at the same time. The leading edge of the diffusion flame moved along with the tip of the enlarging fuel duct, and for this reason the flame spread rate was defined as the velocity of this motion.

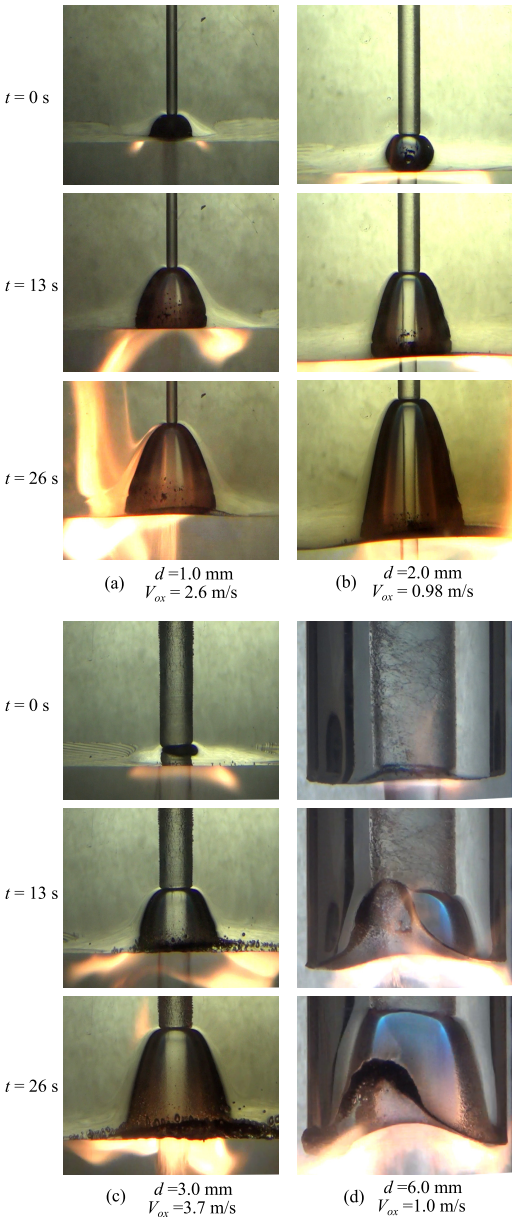

Fig. 2. Pictures of the combustion state with liquid oxygen and PMMA fuel.

The plot in Fig. 3 correlates the flame spread rate with the oxidizer port velocity and fuel port diameter. These errors in Figs. 3 and 4, were calculated from the measurement error of pressure and port diameter. As indicated in the figures, flame spread rate decreases with increasing oxidizer port velocity. Flame spread rate also increases with increasing port diameter, however the sensitivity in port diameter decreases. The flame spread rate of the tests in this study is roughly twenty times

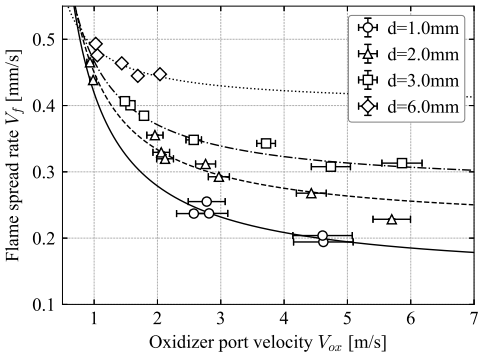

Fig. 3. Flame spread rate decreases with increasing oxidizer velocity and decreasing port diameter.

lower than that reported for tests employing gaseous oxygen as the oxidizer under a similar range of oxidizer port velocities [5]. To summarize the main features of the combustion observed between liquid oxidizer and solid PMMA in this study, we can say that the fuel regresses in the axial and radial directions simultaneously, the port exit diameter is enlarged and the flame spread rate is equivalent to fuel regression rate in axial direction. For these reasons, it seems reasonable to conclude that the combustion of liquid oxygen with a solid fuel duct can be classified as stabilized combustion as defined in previous studies using gaseous oxygen. The empirical formula for flame spread rate V_f [m/s] using gaseous oxygen was identified in a previous study [8] as the following equation:

$$V_f = (C_1/V_{ox} + C_2)P^n \tag{1}$$

V_{ox} [m/s] and P [Pa] are oxidizer port velocity and ambient pressure, respectively. The empirical constants C_1, C_2 and n were determined to be 1.34×10^{-7}, 1.61×10^{-9}, and 0.951, respectively. We try applying this empirical formula to the stabilized combustion with liquid oxygen observed in this study. In this analysis, ambient pressure, P, is atmospheric pressure: 0.1013 MPa; and pressure exponent, n, is assumed to be unity [8], [9]. In addition, experimental values C_1 and C_2, which are constant when using gaseous oxygen, are defined with respect to each port diameter because the flame spread rate in liquid oxygen is influenced by the port diameter. The lines in Fig. 3 show the curves fitted according to Eq. (1). As indicated in the figure, these curves agree well with the trend in the experimental data. Table 1 shows the experimental values, C_1 and C_2, with liquid oxygen. Figure 4 shows the relations of experimental values C_1 and C_2 to port diameter. While C_1 tend to increase, C_2 tend to decrease as port diameter

Table 1. Experimental value: C_1, C_2

Port diameter	Experimental value	
d [mm]	$C_1 \times 10^{-9}$	$C_2 \times 10^{-9}$
1.0	2.8	1.4
2.0	2.38	2.10
3.0	1.91	2.79
6.0	0.88	4.00

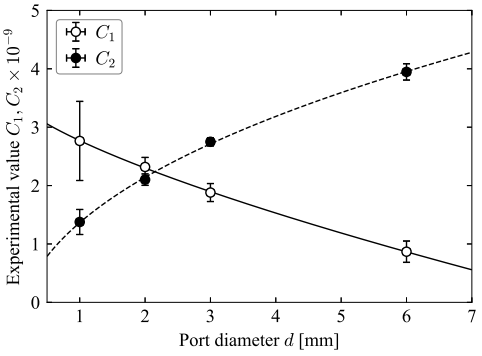

Fig. 4. Relation of experimental values, C_1 and C_2, to port diameter.

increases. Assuming these values can be described by a power function of port diameter, d, they are given by as:

$$C_1 = (-104d^{0.715} + 3.55) \times 10^{-9} \tag{2}$$

$$C_2 = (43.4d^{0.426} - 0.905) \times 10^{-9} \tag{3}$$

where port diameter, d, is in units of [m].

There are two clear differences between the results of tests using liquid oxygen and those using gaseous oxygen. One is the influence of port diameter on flame spread rate. In stabilized combustion with gaseous oxygen, there is no influence of port diameter [8]. The other is the absence of flame spreading combustion; namely, when fully liquid-phase oxygen is supplied, the diffusion flame does not spread into the fuel port even when the oxidizer port velocity is relatively low. When the void ratio of the oxygen is very high, such as in an annular mist flow, the flame spreading combustion mode can be observed. These two differences are discussed in more detail in the following sections.

3.2. Extinction and abnormal regression

When oxidizer port velocity was high and fuel port diameter was small, abnormal fuel regression was observed, and sometimes extinction occurred. Figure 5 (a) shows an example of abnormal fuel regression. The

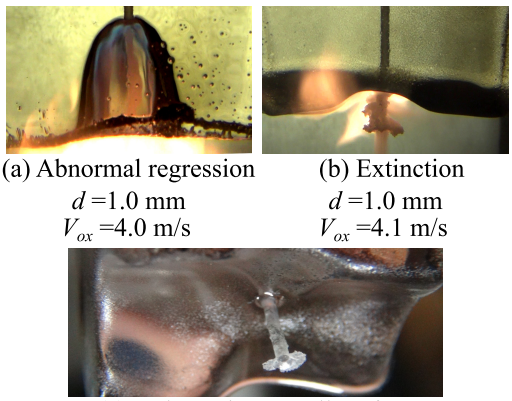

(a) Abnormal regression
d =1.0 mm
V_{ox} =4.0 m/s

(b) Extinction
d =1.0 mm
V_{ox} =4.1 m/s

(c) Unburnt inner wall surface of fuel port after firing (b)

Fig. 5. Pictures of abnormal regression and extinction.

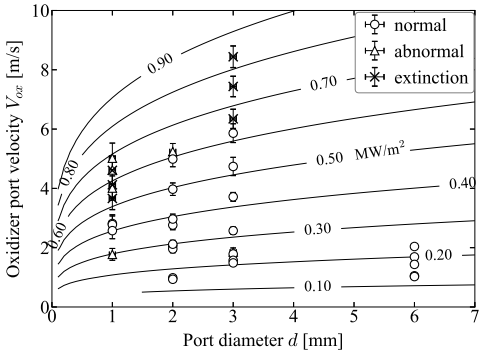

Fig. 6. Abnormal regression and extinction were occur when heat loss, $\dot{q}_{cool}$, is greater than 0.6 W/m^2

fuel regression shape in this figure is noticeably different from the normal regression shape shown in Fig. 2. When abnormal regression occurred, radial regression rate increased and the bell-shape opened wider than in the case of normal regression. Figure 5 (b) shows an example of extinction. In this figure, the inner wall of the fuel port remains unburnt, and the liquid oxygen that spouts out from the bottom spreads around the outer surface of the unburnt inner wall promoting a predominately radial regression. Figure 5 (c) shows the picture of a burnt surface after the firing of (b). As shown in these pictures, the inner wall surface of fuel port remained intact even though it was directly heated by the diffusion flame as shown in (b). It can be inferred that the inner wall surface of the fuel port was not able to vaporize because of the strong cooling effect of the core liquid oxygen flow. When the cooling effect exceeds a certain level, it seems that the inner wall surface of the fuel port is not vaporized, rather it remains as a solid even in the flame region. Liquid oxygen flows through the remaining thin tubular fuel port and flows out from the crack or outlet downstream of the tube. Because the oxygen supply position moves farther from the flame as the fuel burns in the axial direction, either abnormal regression or extinction may occur. Abnormal regression occurs when the oxygen supply is unstable, and extinction occurs when the oxygen supply is insufficient. In other words, abnormal regression and extinction are caused by the same mechanism, although the resulting flame intensity is different.

The following part expresses the relation between extinction and cooling effect. The cooling effect can be calculated as heat loss from the fuel surface to the oxidizer flow, $\dot{q}_{cool}$. The heat transfer between the inner wall surface of the fuel port can be analyzed by treating the oxidizer flow as a turbulent flow without boiling, because sub-cooled boiling at the region right above the tip of an enlarged fuel duct was not observed by high-speed camera and the Reynolds number in these experiments exceeded $Re < 4600$. Thus, the heat loss, $\dot{q}_{cool}$, is expressed as the following equation:

$$\dot{q}_{cool} = Nu_m \lambda_{ox} (\bar{T}_w - T_{ox})/d \tag{4}$$

In Eq. (4), Nu_m, λ_{ox}, $\bar{T}_w$, T_{ox} are the spatially averaged Nusselt number, the heat conductivity of oxidizer, the average wall temperature of the fuel, and the oxidizer temperature, respectively. In this analysis, the average Nusselt number is calculated by the Dittus-Boelter equation [10]:

$$Nu_m = Nu_{m,\infty} = 0.023 Re^{0.8} Pr^{0.4} \tag{5}$$

In Eq. (5), Re and Pr are Reynolds number and Prandtl number, respectively. The calculation of heat loss flux for liquid oxygen uses the following values: a thermal conductivity $\lambda_{ox,LOX}$, of 166×10^{-3} W/m $\cdot$ K; a Prandtl number, Pr_{LOX}, of 2.42; and a kinematic viscosity, ν_{LOX}, of 0.214×10^{-6} m^2/s. An estimated value on average wall temperature of $\bar{T}_{w,LOX} = 120$ K was used because this temperature was found to lead to the best correlation between experimental results and the results calculated by the models derived in the following sections. A previous study in which inner temperatures of a burning fuel were measured was used as a verification of the validity of the average wall temperature selected here [11]. In Fig. 6, contours of heat loss to the oxidizer flow are drawn with plots of each experimental condition. These plots also include the experiments in which the extinction and abnormal regression were observed. The heat loss is calculated according to the Dittus-Boelter equation, Eq. (5). As indicated in the figure, extinction or

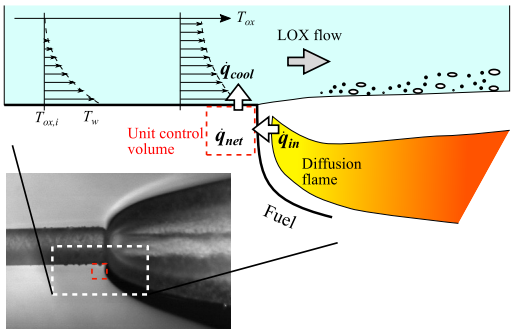

Fig. 7. Schematic of heat balance in a unit volume of fuel.

abnormal regression occur when the oxidizer port velocity is high and the port diameter is small. Equation (5) shows that as the port diameter decreases, heat transfer along the fuel port inner wall surface becomes more active, and thus heat is transferred to the liquid oxygen. On the other hand, the heat transfer from the flame hardly changes regardless of the port diameter. For this reason, it is considered that extinction occurs if the port diameter is too small. The boundary between normal regression and extinction or abnormal regression is located along the heat loss contour of 0.6 $\mathrm{MW/m^2}$. Thus, when heat loss exceeds 0.6 $\mathrm{MW/m^2}$, extinction or abnormal regression occur. For this reason, it can be said that the cooling effect of the oxidizer flow determines the boundary between normal regression and extinction or abnormal regression.

4. Modeling the flame spread rate

4.1. Equations for calculating flame spread rate

A model of the flame spread rate are developed considering the heat balance in a unit volume of fuel. Figure 7 describes a schematic of this model. In this figure, a unit control volume is shown by the square region, which is in contact with both the liquid oxygen flow and the diffusion flame. Only three heat flux terms are considered: heat input from diffusion flame, $\dot{q}_{in}$, heat loss to the oxidizer flow, $\dot{q}_{cool}$, and net heat consumption for heating and vaporizing the fuel, $\dot{q}_{net}$. Here, it is assumed that the heat conduction in the upstream axial and outer radial directions are negligible compared with the quantity of heat input from the diffusion flame and heat loss to the liquid oxidizer in the specified control volume. This assumption is reasonable for a control volume that encompasses the region of steepest thermal gradients, which must be very near the fuel surface when considering that the fuel material has a very low thermal conductivity. Balancing these heat fluxes yields the following equation:

$$\dot{q}_{net} = \dot{q}_{in} - \dot{q}_{cool} \tag{6}$$

Net heat consumption, $\dot{q}_{net}$, an important value for determining the flame spread rate, V_f, is expressed by the following equation:

$$\dot{q}_{net} = V_f \left(\int_{T_i}^{T_{dec}} \rho_f c_{p,f} dT + H_{dec} \rho_f |_{T=T_{dec}} \right) \tag{7}$$

where T_i, T_{dec}, ρ_f, $c_{p,f}$, H_{dec} are the initial fuel temperature, the fuel decomposition temperature, the density of the fuel, the specific heat capacity of the fuel, and the specific decomposition energy, respectively. Assuming a fuel has been precooled, the initial fuel temperature, T_i, in Eq. (7) is the same as the oxidizer temperature. The density and specific heat capacity of PMMA are derived from Ref. [12] as functions of temperature. Stanislav et al. pointed out that the heat of melting is negligible in PMMA until its decomposition [13], so the terms related to melting are eliminated from Eq. (7). The decomposition temperature and specific decomposition energy reported by Stanislav are used in this model. Heat loss, $\dot{q}_{cool}$, can be calculated by Eq. (4). The mechanisms of heat input are complicated because the heat input is the convective heat transfer from the diffusion flame to the solid fuel. In this case, convective heat transfer is affected by buoyancy, oxidizer mass flow rate and the oxidizer vaporization rate, as well as the position of the flame zone above the fuel surface. Therefore, to simplify the discussion, we assume that heat input, $\dot{q}_{in}$, is a constant value, and discuss later in this section the consequences of this simplification. Although the value, $\dot{q}_{in} \sim 1.05$ $\mathrm{MW/m^2}$, is chosen to roughly correspond with the result of experiments, a justification for this value is offered in the section 4.3. Flame spread rate is derived from Eq. (4), Eq. (6) and Eq. (7) to be:

$$V_f = \frac{\dot{q}_{in} - Nu_m \lambda_{ox} d^{-1} \left(\bar{T}_w - T_{ox} \right)}{\int_{T_i}^{T_{dec}} \rho_f c_{p,f} dT + H_{dec} \rho_f |_{T=T_{dec}}} \tag{8}$$

Figure 8 shows the results of calculation using Eq. (8). As can be seen from the figure, the tendency of flame spread rate with respect to oxidizer port velocity and port diameter agrees with most of the experimental results. However, the calculated value of the decrease in flame spread rate resulting from an increase in oxidizer port velocity is different than the experiment value. In the calculation, the rate of decrease is almost constant. Whereas, in the experiments, the rate decreases with increasing oxidizer port velocity before gradually approaching a certain constant value. The reason why

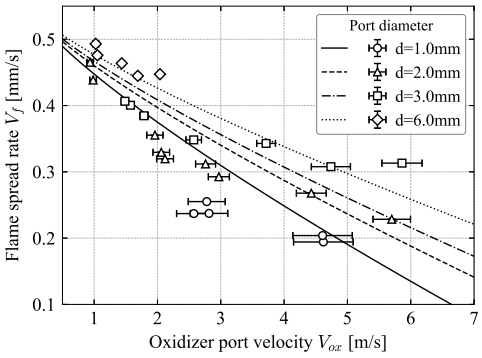

Fig. 8. The flame spread rate calculated by Dittus-Boelter's equation assuming fully developed thermal boundary layer agrees somewhat with the experimental results.

this difference appears is that the heat input from the diffusion flame is assumed to be a constant value that does not depend on the oxidizer port velocity. In reality, the heat input is not constant because it is affected by changes in buoyancy and boundary layer thickness due to changes in the oxidizer port velocity.

4.2. Discussion of model assumptions

Assuming that the flow velocity of vaporized oxygen is equal to the flow velocity of liquid oxygen, the Richardson number, which is the ratio of buoyancy to flow shear, can be used to estimate the buoyancy effect. The Richardson number is defined as the following equation:

$$Ri = g\beta\left(T_f - T_{ox}\right)d/{V_{ox}}^2 \tag{9}$$

Here, g, β, and T_f are the gravitational acceleration, coefficient of thermal expansion, and flame temperature, respectively. The coefficient of thermal expansion, β, for an ideal gas is

$$\beta = -\rho^{-1}\partial\rho/\partial T = \left(T_f + T_{ox}\right)/2T_fT_{ox}. \tag{10}$$

Here, the following values will be assigned: g = 9.8 m/s^2, T_f = 3100 K, T_{ox} = 80 K. Based on these equations, the Richardson number has a maximum value of $Ri \approx 1.1$ when the port diameter is d = 6.0 mm and the oxidizer port velocity is V_{ox} = 1.0 m/s, and minimum value of $Ri \approx 6.2 \times 10^{-3}$ when the port diameter is d = 1.0 mm and the oxidizer port velocity is V_{ox} = 5.0 m/s. From this rough estimation, it can be said that, in most case, the effect of buoyancy can be neglected because $Ri < 0.1$, and the model should take the buoyancy effect into account only when the oxidizer port velocity is low and port diameter is large. Increasing the oxidizer port velocity increases the heat input, because the boundary layer, where the diffusion flame is formed, becomes thinner and the distance between the diffusion flame and the fuel surface decreases. In addition, there is room to improve on the heat loss estimation by Eqs. (4) and (5). This model calculates the Nusselt number assuming the boundary layer of liquid oxygen is fully developed. Although the trend in results will not change qualitatively, it may be more appropriate to implement a Nusselt number correlation corresponding to a developing flow rather than that of a fully developed flow, because the fuel port length is too short for the flow to be fully developed. If the model implemented a developing flow formula for Nusselt number, the value of V_f calculated by the model would decrease greatly in the low-velocity region where the boundary layer has not developed, but only slightly decrease in the high-velocity region where the boundary layer has developed to some extent, because the steeper temperature gradient in the liquid oxygen in the low-velocity region enhances the cooling effect. Currently, there is no Nusselt number correlation from previous research which clearly applies to the flow conditions of our experiments. The accuracy of the model proposed in this paper may be improved by taking these mechanisms in to account. The authors would like to work on these improvements in subsequent research, because these modifications to the model are out of the scope of this paper and related experiments.

4.3. Influence of port diameter on flame spread rate

In this section, the cause of the difference in the influence of port diameter on flame spread rate between gaseous and liquid oxygen is modeled by considering the influence of port diameter on flame spread rate. It is possible to estimate the value of heat input from the heat balance in Eq. (6) by calculating the net heat consumption using Eq. (7) based on experimental flame spread rates determined by Eq. (1) and heat loss flux determined by Eq. (4). Figures 9 and 10 show each heat flux term and the flame spread in liquid and gaseous oxygen, respectively, when the port diameter is 1.0 mm. The estimation for gaseous oxygen uses the following values: an initial temperature, T_i, and oxidizer temperature, T_{ox}, of 280 K; a thermal conductivity, $\lambda_{ox,GOX}$, of 24.7×10^{-3} W/m $\cdot$ K; a Prandtl number, Pr_{GOX}, of 0.725; and a kinematic viscosity, ν_{GOX}, of 14.2×10^{-6} m^2/s. An average fuel wall temperature, $\bar{T}_{w,GOX}$, is assumed approximately 473 K with reference to the measurement results of the surface temperature of burning PMMA by Y.kudo et al. in Ref. [11].

The range of oxidizer port velocities considered with gaseous oxygen is from 20 to 40 m/s to match the range

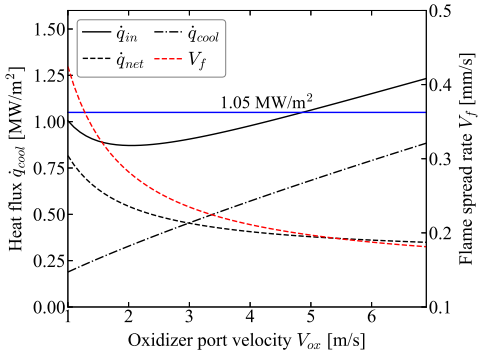

Fig. 9. Heat loss is a half of heat input with liquid oxygen (d=1.0 mm).

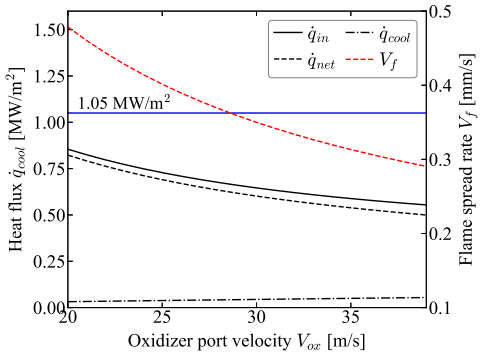

Fig. 10. The proportion of heat loss to heat input is less than 5% with gaseous oxygen (d = 1.0 mm).

of flame spread rates more closely to those with liquid oxygen, and because stabilized combustion with gaseous oxygen is not possible under lower oxidizer port velocities. As indicated in these figures, the estimated values of heat input with liquid oxygen, 0.9 to 1.3 MW/m^2, and that of gaseous oxygen, 0.6 to 0.8 MW/m^2, are close to one other and both approximate the value used in the model; 1.05 MW/m^2 in section 4.1. Therefore, the value of heat input used in the model is a reasonable order of magnitude. The proportion of heat loss to heat input with gaseous oxygen is less than 5%, and the effect of it on this estimation can be neglected; however, that with liquid oxygen is 50% or more. To quantitatively evaluate the magnitude of influence of port diameter on flame spread rate, we introduce a partial derivative of flame spread rate with respect to port diameter, $\partial V_f/\partial d$. When Eq. (8) is partially differentiated, the heat input term, $\dot{q}_{in}$, is cancelled out and the partial derivative can be expressed as following

Table 2. Parameter ratio of gaseous oxygen to liquid oxygen and the exponent values.

Parameter ratio	Values of ratio	Exponent of parameter
$\lambda_{ox,GOX}/\lambda_{ox,LOX}$	0.15	1
Pr_{GOX}/Pr_{LOX}	0.30	0.4
ν_{GOX}/ν_{LOX}	66	-0.8
$\frac{(\bar{T}_w - T_{ox,GOX})}{(\bar{T}_w - T_{ox,LOX})}$	5	1
Net heat consumption per unit volume	0.89	1

equation:

$$\frac{\partial V_f}{\partial d} = \frac{0.0046\lambda_{ox} Pr^{0.4}\nu^{-0.8}\left(\bar{T}_w - T_{ox}\right){V_{ox}}^{0.8} d^{-1.2}}{\int_{T_i}^{T_{dec}} \rho_f c_{p,f} dT + H_{dec}\rho_f|_{T=T_{dec}}} \tag{11}$$

Where ν is the kinematic viscosity of the oxidizer. Note that of the exponents of V_{ox} and d in Eq. (11), that of V_{ox} is positive and slightly less than one while that of d is negative and slightly larger than one. This equation explains the decrease in sensitivity of flame spread rate to changes in port diameter or oxidizer port velocity when the values of these parameters are relatively large. In the case of liquid oxygen, the magnitude of this tendency ranges from 2.26×10^{-3} to 9.21×10^{-2} s^{-1} when the oxidizer port velocity ranges from 1.0 to 7.0 m/s and port diameter ranges 1.0 to 6.0 mm. On the other hand, the magnitude of this tendency when gaseous oxygen is used ranges from 3.93×10^{-5} to 1.59×10^{-3} s^{-1}, roughly two orders of magnitude smaller. Table 2 shows the ratios of each parameter of gaseous oxygen to liquid oxygen and the exponents of each parameter in Eq. (11). Net heat consumption per unit volume is equivalent to the denominator of Eq. (11). This table shows that the kinematic viscosity of the oxidizer is the most influential factor on the influence of port diameter in the comparison of liquid versus gaseous oxygen, and that the cumulative impact of the other parameters combined is less than ten percent that of the kinematic viscosity parameter. In fact, since the range of oxidizer port velocities where stabilized combustion is established should exceed approximately 20 m/s when gaseous oxygen is used [14], the velocity is around ten times higher than that considered in the above calculation. For this reason, the influence observed in actual experiment with gaseous oxygen should be roughly a tenth of that when liquid oxygen is used.

5. Conclusion

In this study, combustion state and flame spread rate opposed to liquid oxygen flow in a fuel duct were experimentally investigated. Several firing tests show that stabilized combustion may be sustained using liquid oxygen as an oxidizer. The flame spread rate decreases as the oxidizer port velocity increases and port diameter decreases, and the empirical formula of flame spread rate was obtained. Extinction and abnormal regression occur when oxidizer port velocity is high and port diameter is small. It can be concluded that the cooling of the fuel by the oxidizer flow in this configuration has a strong effect on the combustion when liquid oxygen is used. Models of flame spread rate developed considering the heat balance of three heat fluxes at the fuel surface are in good agreement with the experimental results. However, there is room for improvement regarding the effects of buoyancy and the boundary layer of the combustion gas flow on heat input, and the effect of the development of the temperature boundary layer in the liquid oxygen flow on the heat loss due to cooling. Sensitivity analysis revealed that the primary reason why the influence of port diameter appears when liquid oxygen is used but not when gaseous oxygen is used is that the cooling rate at the fuel surface is greatly increased due to the larger kinematic viscosity of liquid oxygen.

Acknowledgments

This work was supported in part by JSPS KAKENHI Grant Number 19K04832.

References

[1] H. Nagata, H. Teraki, Y. Saito, R. Kanai, H. Yasukochi, M. Wakita, T. Totani, Verification Firings of End-Burning Type Hybrid Rockets, Journal of Propulsion and Power 33 (2017) 1473–1477.

[2] M. A. Hitt, R. A. Frederick, Testing and Modeling of a Porous Axial-Injection, End-Burning Hybrid Motor, Journal of Propulsion and Power 32 (2016) 834–843.

[3] F. Lastrina, R. Magee, R. McAlevy, Flame spread over fuel beds: solid-phase energy considerations, Symposium (International) on Combustion 13 (1971) 935–948.

[4] A. Fernandez-Pello, F. A. Williams, Laminar flame spread over PMMA surfaces, Symposium (International) on Combustion 15 (1975) 217–231.

[5] N. Hashimoto, S. Watanabe, H. Nagata, T. Totani, I. Kudo, Opposed-flow flame spread in a circular duct of a solid fuel: Influence of channel height on spread rate, Proceedings of the Combustion Institute 29 (2002) 245–250.

[6] T. Matsuoka, S. Murakami, H. Nagata, Transition characteristics of combustion modes for flame spread in solid fuel tube, Combustion and Flame 159 (2012) 2466–2473.

[7] T. Takei, T. Tsutomu, T. Sakurai, Burning characteristics of LOx vaporizatin preburner for A-SOFT HR engines (in Japanese), in: Proceedings of 60th Space Sciences and Technology Conference, Japan Society for Aeronautical and Space Sciences, Hakodate, Japan, 2016, p. 4A06.

[8] N. Hashimoto, End-burning type hybrid rocket, Ph.D dissertation (in Japanese), Ph.D. thesis, Hokkaido University, Sapporo, Japan, Sapporo, 2004.

[9] Y. Saito, M. Kimino, A. Tsuji, Y. Okutani, K. Soeda, H. Nagata, High Pressure Fuel Regression Characteristics of Axial-Injection End-Burning Hybrid Rockets, Journal of Propulsion and Power (2019) 1–14.

[10] F. W. Dittus, L. M. Boelter, Heat transfer in automobile radiators of the tubular type, International Communications in Heat and Mass Transfer 12 (1985) 3–22.

[11] Y. Kudo, M. Itakura, Y. Fujita, A. Ito, Flame spread and extinction over thermally thick PMMA in low oxygen concentration flow, Fire Safety Science (2005) 457–468.

[12] W. Wunderlich, in: J. Brandrup, E. H. Immergut, E. A. Grulke, A. Abe, D. R. Bloch (Eds.), Plymer Handbook, volume 12, Wiley, NewYork, 4 edition, 1990, p. 265.

[13] S. I. Stoliarov, R. N. Walters, Determination of the heats of gasification of polymers using differential scanning calorimetry, Polymer Degradation and Stability 93 (2008) 422–427.

[14] N. Hashimoto, H. Nagata, T. Totani, I. Kudo, Determining factor for the blowoff limit of a flame spreading in an opposed turbulent flow, in a narrow solid-fuel duct, Combustion and Flame 147 (2006) 222–232.